

# A high-precision model of first-order reversal curve (FORC) functions for single-domain ferromagnets with uniaxial anisotropy

Andrew J. Newell

*Center for Research in Scientific Computation, Department of Marine,  
Earth and Atmospheric Sciences, P.O. Box 8208,  
North Carolina State University, Raleigh, NC 27695-8208\**

Plots of the first-order reversal curve (FORC) function are used to characterize ferromagnetic particles in rocks. The function is based on classical Preisach theory, which represents magnetic hysteresis by elementary loops with displacement  $H_u$  and half width  $H_c$ . Using analytical and numerical integration of single-particle magnetization curves, a high-precision FORC function is calculated for a sample with randomly oriented, noninteracting, elongated single-domain particles. Some properties of the FORC function are independent of the distribution of particle orientations and shapes. There is a negative peak near the  $H_u$  axis and the FORC function is identically zero for  $H_u > 0$ . The negative peak, previously attributed to particle interactions, is due to the increasing slope of a reversible magnetization curve near a jump. This peak is seen in experimental FORC functions of SD samples but not of samples with larger particles, probably because of Barkhausen jumps. The second feature is not seen in any experimental FORC function. A spread of the function to  $H_u > 0$  can be caused by particle interactions and nonuniform magnetization.

*An edited version of this paper was published by AGU. Newell, A. J. (2005), A high-precision model of first-order reversal curve (FORC) functions for single-domain ferromagnets with uniaxial anisotropy, *Geochem. Geophys. Geosyst.*, 6, Q05010, doi:10.1029/2004GC000877. To view the published open abstract, go to <http://dx.doi.org> and enter the DOI.*

## I. INTRODUCTION

Rock magnetists, paleomagnetists and environmental magnetists use magnetic hysteresis measurements to characterize ferromagnetic minerals in rocks and sediments. Many labs represent the hysteresis by a few well-known parameters: the saturation magnetization  $M_s$ , the saturation remanence  $M_{rs}$ , the coercivity  $H_c$ , and the coercivity of remanence  $H_{rc}$ <sup>7</sup>. These parameters can be summarized in a plot of  $M_{rs}/M_s$  against  $H_{rc}/H_c$ <sup>3</sup>. This “Day” plot is a standard tool for estimating mineral size, but its interpretation is highly ambiguous. One reason for ambiguity is that samples are often mixtures of simpler components. Suites of samples with varying ratios of components often follow trends on the Day plot<sup>5,6,16,26,39</sup>. However, each sample is represented by only one data point. This provides little information on the components, which are themselves collections of particles with distributions of physical properties. More detailed information on each sample can be obtained using isothermal remanence curves, which can be considered one-dimensional profiles through the hysteresis<sup>9,33</sup>. Plots of Preisach or FORC functions provide two-dimensional profiles<sup>4,8,12,29</sup>.

The FORC function is a measure of the rate of irreversible change in magnetization. It is determined by a set of magnetization curves called first-order reversal curves (FORCs), as in Fig. 1a. Where there is no hysteresis it is zero. The relationship between FORCs and

FORC functions is derived in classical Preisach theory<sup>18</sup>, where the latter is called the Preisach function or distribution. The same relationship can still be used to determine the FORC function even where the theory does not apply (but see Section II A). Users of the FORC function attempt to identify multiple components in a sample<sup>32</sup> and compare the components with FORC plots for relatively well-characterized samples<sup>22,29</sup>.

The FORC function has mainly been used to obtain qualitative information on the components. Although there has been some theoretical modeling of FORC functions<sup>29,30,37</sup>, quantitative predictions have not been compared with experiment. Most FORC plots do not even have scale bars on them. The magnitude of the FORC function is not very meaningful unless the volume of the magnetic component is known. However, if there is only one component the magnetization and field can be normalized as in Fig. 1a to get a normalized FORC function.

The magnetic tape in Fig. 1a is probably composed of elongated particles of maghemite or cobalt-doped maghemite<sup>19</sup>. (Unfortunately, the details are proprietary.) Perpendicular to the tape, the ratio of saturation remanence to saturation magnetization is  $M_{rs}/M_s = 0.62$ , indicating that the particles are single-domain (SD) with some anisotropy to their orientations (Section III C). SD particles play a central role in rock magnetism<sup>7</sup> and rocks with elongated SD particles are particularly useful for paleomagnetism because they carry a stable natural remanent magnetization (NRM). These include magnetite inclusions in pyroxenes<sup>10</sup>, plagioclase<sup>34</sup> and ash flow tuffs<sup>32,41</sup>. As described in Section II A, the FORC function for SD particles has several distinct features, none of which have been fully explained.

In this article I calculate FORC functions for systems of single-domain particles with uniaxial anisotropy. The calculations include the effects of random distributions of particle orientations (isotropic or anisotropic) and dis-

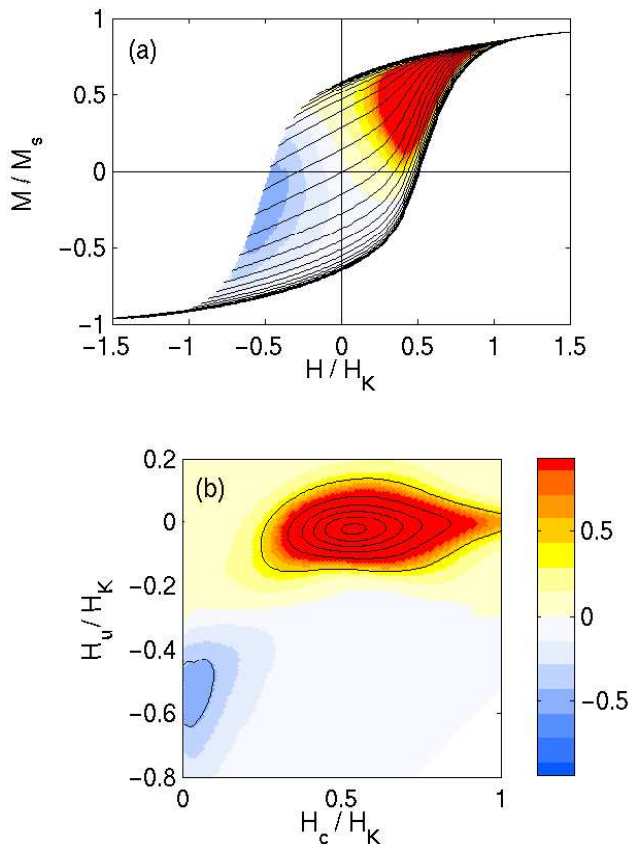


FIG. 1: Two views of the FORC function. (a) Black lines: first-order reversal curves (FORCs) for a high-density magnetic tape (courtesy of Chris Pike). Magnetic fields are normalized by  $H_K$ , the field at which the loop closes. The magnetic moment is normalized by the saturation magnetization  $M_s$ . For clarity, only a subset of the 140 curves are shown. Color image: the normalized FORC function (derived using a method similar to that described in<sup>29</sup>). The top of the color scale is truncated to make the negative region visible. (b) The FORC function redrawn in normalized  $(H_c, H_u)$  coordinates. The color scale is restricted to  $[-1, 1]$  to emphasize the negative region. The black contours are six times farther apart than the color contours and cover the entire range of  $\mu$ . No data were collected in the white region.

tributions of particle shapes. A lot of the work is carried out analytically, allowing high-accuracy calculations. I also use the analytical expressions to explain the main features of the FORC function in terms of the component particles. And I compare the theory to experimental FORC functions.

## II. BACKGROUND

In this section I describe some of the theory behind the FORC function and some previous work on FORC functions in single-domain systems. Then I describe the classic model for single-domain particles, the Stoner-

Wohlfarth model. This model is the starting point for the calculations in the Section III.

### A. The FORC function

There are two common ways of measuring the FORC function (Fig. 2). Most paleomagnetists decrease the field from a large positive field to a minimum field  $H'_a$  and then measure the magnetization at an increasing series of fields  $H'_b$  (The FORCs in Fig. 1a were measured this way). A set of measurements  $M(H'_a, H'_b)$ , with fixed  $H'_a$  and  $H'_a \leq H'_b$ , is called an increasing FORC<sup>18</sup>. Most physicists and engineers use decreasing FORCs ( $M(H''_a, H''_b)$  in Fig. 2), which start at negative saturation.

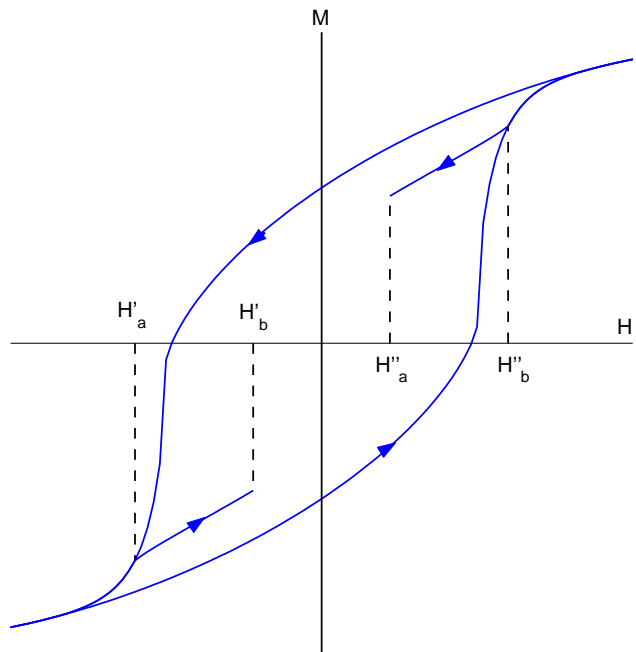


FIG. 2: Two types of first-order reversal curves. An increasing FORC is the curve  $M(H'_a, H'_b)$ , with  $H'_a$  fixed and  $H'_b > H'_a$ . A decreasing FORC is  $M(H''_a, H''_b)$  with  $H''_b$  fixed and  $H''_a < H''_b$ .

<sup>18</sup> showed that the FORC function can be derived from the FORCs using

$$\mu(H_a, H_b) = -\frac{1}{2} \frac{\partial^2 M(H_a, H_b)}{\partial H_a \partial H_b} \quad (1)$$

for increasing FORCs, or

$$\mu(H_a, H_b) = \frac{1}{2} \frac{\partial^2 M(H_a, H_b)}{\partial H_a \partial H_b} \quad (2)$$

for decreasing FORCs. If classical Preisach theory correctly predicts the hysteresis of the sample, the two functions are equal (Section IV B), but in general they are different. Unless I state otherwise, I use “FORC function” to refer to the increasing FORC function.

The FORC function is often converted to  $(H_c, H_u)$  coordinates, where  $H_u = (H_b + H_a)/2$  and  $H_c = (H_b - H_a)/2$ . In some publications  $\mu$  is multiplied by a factor of two, but I use the same  $\mu$  for both sets of coordinates. Since it is simpler to derive expressions for  $\mu(H_a, H_b)$  and trivial to convert to  $\mu(H_c, H_u)$ , I mostly give explicit expressions in terms of  $H_a$  and  $H_b$ .

Many Preisach modelers make *a priori* assumptions about the form of the FORC function. A common one<sup>8</sup> is that it can be expressed as the product of two independent functions,  $\mu(H_c, H_u) = P(H_c)Q(H_u)$ , with  $Q(H_u)$  representing interactions between particles. It is often further assumed that  $P$  and  $Q$  are proportional to normal probability density functions<sup>35,40</sup>. Until recently it was hard to judge such assumptions because the only plots of the FORC function were plots of the *a priori* function with parameters fitted to the data.

<sup>29</sup> estimate the FORC function using fits of  $M(H_a, H_b)$  to piecewise polynomials. This allows direct comparisons between the function and the assumptions of Preisach modelers. For example, the FORC function in Fig. 1a cannot be a probability distribution because it is negative over much of the left half of the hysteresis loop. Similar negative regions are seen in other single-domain samples<sup>1,28,29</sup>.

If the FORC function is plotted in  $(H_c, H_u)$  coordinates (Fig. 1b), the negative region rises to a ridge along the negative  $H_u$  axis and the positive region peaks near the positive  $H_c$  axis. The negative and positive regions are at the same distance from the origin, but the positive peak is higher.

Negative regions have been attributed to particle interactions<sup>29,37</sup>. However,<sup>21</sup> also see them in numerical models of noninteracting single-domain particles, so particle interactions can not be the sole reason for the negative regions.<sup>21</sup> attribute the negative region to a systematic decrease, for a given  $H_b < 0$ , in the slopes of the FORCs as  $H_a$  decreases. However, it is not clear why this decrease occurs or why similar negative regions are not seen in non-SD samples.

The FORC function has other features that have not been adequately explained. Why are the positive and negative regions roughly symmetric about the  $H_u = -H_c$  axis but so different in magnitude? Also, the positive region in<sup>21</sup> (their Fig. 2) has a boomerang shape. (The negative region probably has a boomerang shape as well, but the axes do not extend far enough.) Why does the boomerang have a 135° internal angle? And why is this shape not seen in the experimental FORC diagram (Fig. 1b)? In this article I answer these questions by relating the FORC function for a large number of particles to the magnetic hysteresis of the component particles.

## B. The Stoner-Wohlfarth Model

The model of<sup>38</sup> predicts the magnetic hysteresis for single-domain particles with a uniaxial anisotropy (hav-

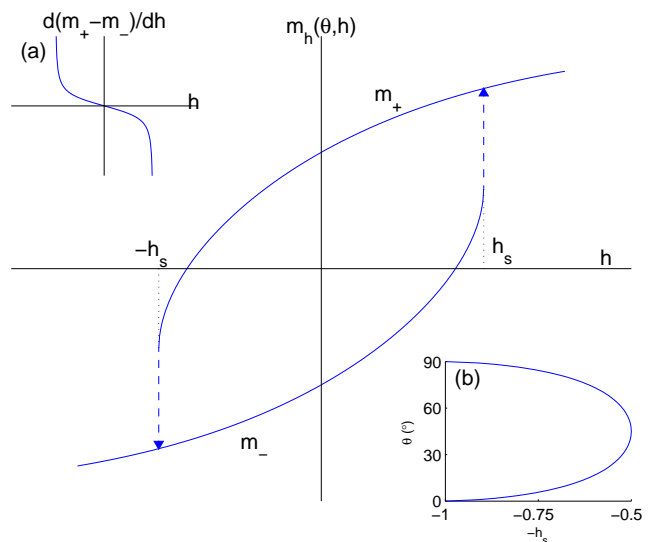


FIG. 3: Main plot: The solid curves are the stable solutions  $m_{\pm}$  of the Stoner-Wohlfarth model for an angle  $\theta = 60^\circ$ . The jumps at the switching fields  $\pm h_s$  are shown as dashed lines with arrows indicating the directions of the jumps. Inset (a): Difference between the derivatives of the solution curves ( $D_h f = d/dh(m_+ - m_-)$ ). This difference is zero for  $|h| > h_s$ . Inset (b): The relationship between switching field and the angle  $\theta$  between field and easy axis.

ing a single preferred axis for magnetization in zero field).

Let  $\theta$  be the acute angle between the field and the easy axis. Let  $\phi$  be the angle between the positive field direction and the magnetization. The energy for a given pair of angles  $\theta$  and  $\phi$  is (in SI units)

$$E = K_u V \sin^2(\phi - \theta) - \mu_0 M_s H V \cos \phi, \quad (3)$$

where  $K_u$  is a parameter representing the magnitude of the anisotropy. This can have more than one physical origin. If the anisotropy is a magnetostatic anisotropy due to particle elongation then  $K_u = (1/2)\mu_0 N M_s^2$ , where  $N$  is the shape-dependent demagnetizing factor (see Appendix A) and  $M_s$  the saturation magnetization. The magnetization in the direction of the field is  $M_h = M_s \cos \phi$ .

Define an anisotropy field  $H_K = 2K_u/\mu_0 M_s$ , a reduced field  $h = H/H_K$ , and a reduced energy

$$\eta = \frac{1}{2} \sin^2(\phi - \theta) - h \cos \phi. \quad (4)$$

For a given field angle  $\theta$  an equilibrium solution for  $\phi$  satisfies

$$d\eta/d\phi = -\frac{1}{2} \sin(2\phi - 2\theta) + h \sin \phi = 0 \quad (5)$$

and it is stable if  $d^2\eta/d\phi^2 > 0$ . There are two solution curves  $m_h = M_h/M_s = m_{\pm}(\theta, h)$  for the stable state (e.g., Fig. 3).

When the magnetization reaches the end of the upper curve it becomes unstable and jumps to the lower

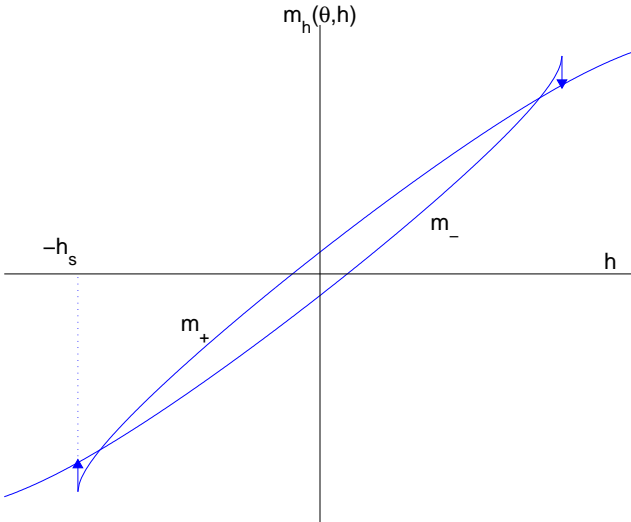


FIG. 4: Hysteresis of a Stoner-Wohlfarth particle with  $\theta = 85^\circ$ . The solution curves cross each other and the jump at  $h = -h_s$  is upward.

curve. The magnitude of the field at which this occurs, the switching field, is<sup>38</sup>

$$h_s = \frac{\sqrt{1 - t^2 + t^4}}{1 + t^2}, \quad (6)$$

where  $t = \tan^{1/3} \theta$ .

If the function  $h = h_s(\theta)$  is inverted, one gets the function  $\theta = h_s^{-1}(h)$  shown in Fig. 3b. It has two branches meeting at  $\theta_s(\pi/4) = -1/2$ . The two branches are given by  $\theta_s(h)$  and  $\pi/2 - \theta_s(h)$ , where<sup>38</sup>

$$\theta_s(h) = h_s^{-1}(h) = -\arctan \left[ \frac{\sqrt{3} - \sqrt{4h^2 - 1}}{2\sqrt{1 - h^2}} \right]^3. \quad (7)$$

Aside from the special cases  $\theta = 0$  and  $\theta = \pi/2$ , the slope  $dm_+/dh$  approaches infinity as the field approaches the jump. An expression for this slope can be obtained using the chain rule:  $dm_+/dh = (dm_+/d\phi)/(d\phi/dh)$ . To get  $dh/d\phi$ , solve (5) for  $h$  and take the derivative with respect to  $\phi$ . Since  $m_+ = \cos \phi$ ,

$$\frac{dm_+}{dh} = \frac{2 \sin^3 \phi}{2 \cos(-2\phi + 2\theta) \sin \phi + \sin(-2\phi + 2\theta) \cos \phi}. \quad (8)$$

The difference between the slopes of the upper and lower curves is plotted in Fig. 3a. The difference is zero for  $|h| > h_s$ , while for  $-h_s < h < h_s$  it goes from  $+\infty$  to  $-\infty$  as  $h$  increases.

The jump in magnetization at the switching field is generally downward, but for  $\theta > 76.72^\circ$  it is upward<sup>38</sup> (p.621). An example of an upward jump is shown in Fig. 4. Before the jump the curves  $m_+$  and  $m_-$  cross each other, so “upper” and “lower” trade places.

In real units, the switching fields range from  $0.5H_K$  to  $H_K$ . Thus, in a set of randomly oriented Stoner-Wohlfarth particles, the collective hysteresis loop closes at  $H = H_K$  (compare Fig. 1a). If all easy axis directions are equally likely the saturation remanence is  $0.5M_s$  and the coercivity is  $0.479H_K$ <sup>38</sup>.

### III. RESULTS

In this section I derive the (increasing) FORC function for increasingly complex systems of Stoner-Wohlfarth particles. These are a single oriented particle (Section III A), randomly oriented identical particles (isotropic in Section III B and anisotropic in Section III C), and randomly oriented particles with a distribution of shapes (Section III D).

#### A. Single Particle

For a single particle or a set of identical particles one can normalize the fields as in Section II B and define a normalized FORC function

$$\tilde{\mu}(h_a, h_b; \theta) = \frac{H_K^2}{M_s} \mu(H_a, H_b; \theta), \quad (9)$$

where  $h_a = H_a/H_K$  and  $h_b = H_b/H_K$ . The semicolon before  $\theta$  indicates that  $\theta$  is a fixed parameter for a given particle. Then

$$\tilde{\mu}(h_a, h_b; \theta) = -\frac{1}{2} \frac{\partial^2 m_h}{\partial h_a \partial h_b}. \quad (10)$$

Consider a Stoner-Wohlfarth particle with angle  $\theta$  between field and easy axis (Fig. 3). If the field starts at a large positive value, decreases to  $h_a$ , and then increases to  $h_b$ , the magnetization is given by

$$m_h(\theta, h_a, h_b) = \begin{cases} m_+(\theta, h_b) & \text{if } h_a > -h_s(\theta) \text{ or } h_b > h_s(\theta), \\ m_-(\theta, h_b) & \text{if } h_a < -h_s(\theta) \text{ and } h_b < h_s(\theta). \end{cases} \quad (11)$$

Note that  $m_h$  is not defined at the discontinuities ( $h_a = -h_s$  and  $h_b = h_s$ ).

This can be expressed in terms of the Heaviside function  $\Theta(x)$ , which is defined as  $\Theta(x) = 0$  for  $x < 0$  and  $\Theta(x) = 1$  for  $x > 0$  and is undefined for  $x = 0$ :

$$m_h(\theta, h_a, h_b) = m_+(\theta, h_b) [1 - \Theta(-h_a - h_s)\Theta(-h_b + h_s)] + m_-(\theta, h_b)\Theta(-h_a - h_s)\Theta(-h_b + h_s). \quad (12)$$

Then, since  $\partial\Theta(-h_a - h_s)/\partial h_a = -\delta(h_a + h_s)$ ,

$$\frac{\partial m_h}{\partial h_a}(\theta, h_a, h_b) = \delta(h_a + h_s)\Theta(-h_b + h_s)f(\theta, h_b), \quad (13)$$

where  $\delta(x)$  is the Dirac delta function and  $f(\theta, h) \equiv m_+(\theta, h) - m_-(\theta, h)$  is the difference between the upper and lower curves.

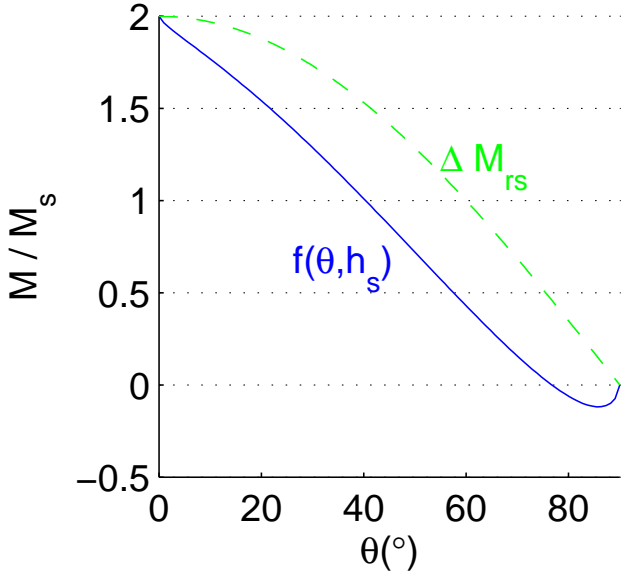


FIG. 5: The jump in magnetization at the switching field as a function of easy axis direction. For comparison, the difference between positive and negative remanence ( $\Delta M_{rs} = 2 \cos \theta$ ) is also plotted.

The value of  $f(\theta, h)$  at  $h = h_s$  is the size of the jump from the lower curve to the upper curve. At  $\theta = 0$  this is equal to 2, the difference between positive and negative saturation (since the magnetization is normalized by  $M_s$ ). As  $\theta$  increases the magnitude of the jump decreases (Fig 5). At angles of  $\theta$  near  $\pi/2$  it is negative, as in Fig. 4.

Taking the derivative of (13) with respect to  $h_b$  and using (1), we get

$$\begin{aligned} \tilde{\mu}(h_a, h_b; \theta) &= \frac{1}{2} \delta(h_a + h_s) \delta(-h_s + h_b) f(\theta, h_b) \\ &\quad - \frac{1}{2} \delta(h_a + h_s) \Theta(h_s - h_b) D_h f(\theta, h_b). \end{aligned} \quad (14)$$

The first term represents the jump at  $h_b = -h_a = h_s$ , so  $f(\theta, h_b)$  can be replaced by  $f(\theta, h_s)$ . In the other term  $D_h f(\theta, h_b) = \partial f(\theta, h) / \partial h|_{h=h_b}$  is the difference between the slopes of the curves (e.g., Fig. 3a). Each slope is a measure of reversible change, but the difference is the result of a jump from one curve to the other. Information on the slope of either curve by itself is lost.

### B. Average over random orientations (isotropic)

Consider a collection of randomly oriented, identical Stoner-Wohlfarth particles. Assume that all easy axis orientations are equally likely. If  $\tilde{\mu}(h_a, h_b; \theta)$  is the normalized FORC function for a given angle  $\theta$  (equation 14),

the average  $\tilde{\mu}$  is given by the integral over a half sphere:

$$\tilde{\mu}(h_a, h_b) = \int_0^{\pi/2} \tilde{\mu}(h_a, h_b; \theta) \sin \theta d\theta. \quad (15)$$

The integrand  $\tilde{\mu}(h_a, h_b; \theta)$  contains the delta function  $\delta(h_a + h_s)$ . Inside the delta function  $h_a$  is fixed but  $h_s$  is a function of  $\theta$  (equation 6). If we define  $p(\theta) = h_a + h_s(\theta)$ , then<sup>20</sup> (p. 469)

$$\delta(p(\theta)) = \sum_n \frac{1}{|p'(\theta_n)|} \delta(\theta - \theta_n), \quad (16)$$

where  $\theta_n$  are the zeros of  $p(\theta)$  and the prime denotes a derivative. The condition  $p'(\theta_n) \neq 0$  must be satisfied or the delta function is meaningless.

The zeros of  $p(\theta)$  between 0 and  $\pi/2$  lie on the curve in Fig. 3b. For  $-1 < h_a < -0.5$  these are  $\theta_a \equiv \theta_s(h_a)$  and  $\pi/2 - \theta_a$ . The inverse function  $\theta = p^{-1}(h)$  is the solution of  $h = p(\theta)$ . Therefore  $p^{-1}(h) = \theta_s(h - h_a)$  or  $p^{-1}(h) = \pi/2 - \theta_s(h - h_a)$  and  $(p^{-1})'(0) = \pm \theta'_s(-h_a)$ . By (7)  $\theta_s$  is an even function of  $h$ . Using the inverse function theorem<sup>36</sup> (p. 208),

$$\frac{1}{p'(p^{-1}(0))} = (p^{-1})'(0) = \theta'_s(h_a). \quad (17)$$

Combining (16) and (17) we get the required transformation

$$\delta(h_a + h_s) = |\theta'_s(h_a)| (\delta(\theta - \theta_a) + \delta(\theta - \pi/2 + \theta_a)). \quad (18)$$

With this substitution, the result of the integration is

$$\tilde{\mu}(h_a, h_b) = \alpha(h_a) \delta(h_a + h_b) + \beta(h_a, h_b) \Theta(-h_a - h_b), \quad (19)$$

where

$$\alpha(h_a) = \frac{|\theta'_s(h_a)|}{2} \left[ g(\theta_a, h_a) + g\left(\frac{\pi}{2} - \theta_a, h_a\right) \right] \quad (20a)$$

$$\beta(h_a, h_b) = -\frac{|\theta'_s(h_a)|}{2} \left[ D_h g(\theta_a, h_b) + D_h g\left(\frac{\pi}{2} - \theta_a, h_b\right) \right] \quad (20b)$$

$$g(\theta, h) = f(\theta, h) \sin \theta. \quad (20c)$$

These equations only apply in the trapezoidal region  $-1 \leq h_a \leq -1/2$  and  $h_a \leq h_b \leq -h_a$ , outside of which the function is zero.

The original function  $\mu$  can be recovered from  $\tilde{\mu}$  using (9):

$$M_s \mu(H_a, H_b) = A(H_a) \delta\left(\frac{H_a + H_b}{H_K}\right) + B(H_a, H_b) \Theta(-H_a - H_b), \quad (21)$$

where  $A(H_a) = r^2 \alpha(h_a)$ ,  $B(H_a, H_b) = r^2 \beta(h_a, h_b)$ , and  $r = M_s / H_K$ . Multiplying  $\mu$  by  $M_s$  makes it dimensionless.

The coefficients  $A$  and  $B$  are plotted in Fig. 6a.  $A$  has an asymptote at  $H_c = 0.5 H_K$ . This occurs because

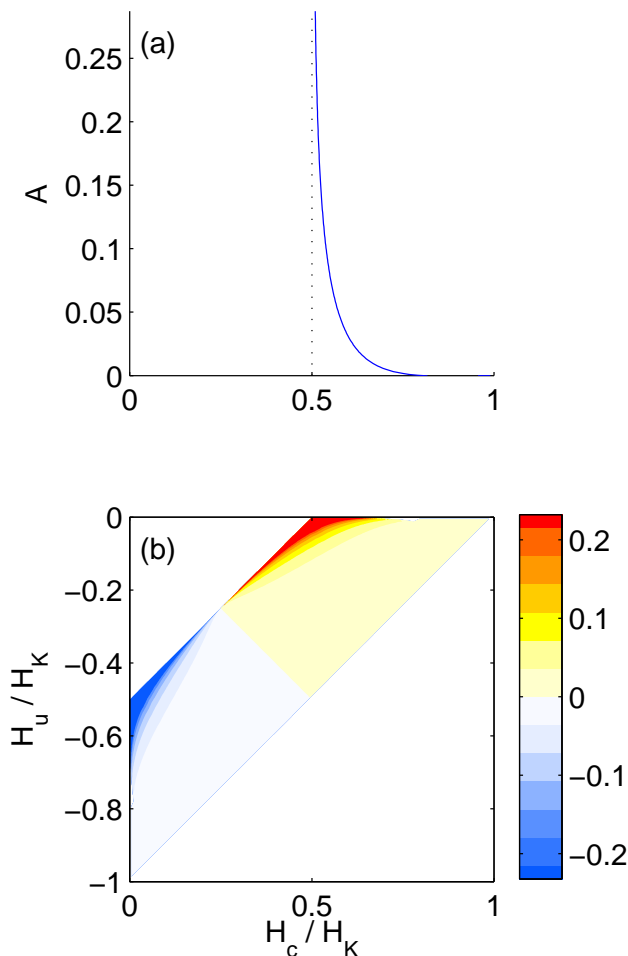


FIG. 6: The FORC function (21) for an isotropic sample of identical particles with aspect ratio  $q = 2$ . It has a continuous part in the region  $H_u < 0$  and a delta function along the  $H_c$  axis. (a) The delta function multiplier  $A$ , representing jumps in magnetization. (b) The continuous part  $B$ , representing changes in the slope of the magnetization curve.  $B$  is zero outside of the colored region. A narrower color scale is used than in Fig. 1b.

the switching fields are concentrated near  $h_a = -1/2$ , and the derivative  $\theta'_s(h)$  approaches infinity at  $h = -1/2$  (Fig. 3b).  $A$  also has a negative region between  $0.806H_K$  and  $H_K$ . This field range corresponds to angles between  $86.5^\circ$  and  $90^\circ$ . This is only part of the range of angles ( $76.72^\circ$  to  $90^\circ$ ) for which the jump at  $h_s$  is negative. The narrowing of the range occurs because the same switching fields are possessed by particles in a complementary range of small angles  $[0^\circ, 22.3^\circ]$ . In these particles the jumps are downward and larger in magnitude than the upward jumps. However, on a sphere small angles of  $\theta$  occupy less solid angle. Thus, downward jumps dominate until the ratio between solid angles offsets the ratio of jump sizes. The negative swing in  $A$  is too small to see in Fig. 6a.

The component  $B$  contains the derivative  $D_h f$  and

therefore represents differences between slopes of the upper and lower curves of each particle. Since the functions  $\sin \theta_a$ ,  $\cos \theta_a$  and  $|\theta'_a|$  are always positive,  $B$  and  $D_h f$  have opposite signs. Near the  $H_u$  axis, as  $H_b$  approaches  $H_a$  the slope of the upper curve approaches infinity while the slope of the lower curve stays finite. Thus,  $B$  approaches negative infinity. Near the  $H_c$  axis the roles are reversed and  $B$  approaches positive infinity. This asymptote is at  $H_b = -H_a$  because the jumps in Stoner-Wohlfarth particles are symmetrically placed about  $H = 0$ . Other kinds of ferromagnets do not have this symmetry.

$B$  has an asymptote at  $H_a = -H_K/2$  for the same reason that  $A$  does. This is a line at a  $45^\circ$  angle with respect to the  $H_u$  and  $H_c$  axes. Away from this line  $B$  has a downward trend.

In summary, the FORC function is concentrated around three lines that meet at  $135^\circ$  angles. One line ( $H_c = 0$ ) is potentially significant beyond the Stoner-Wohlfarth model (Section IV A), one ( $H_u = 0$ ) reflects a symmetry of Stoner-Wohlfarth hysteresis, and one ( $H_a = -H_K/2$ ) comes from the angular dependence of the switching field in the Stoner-Wohlfarth model. The greatest concentration is around the two meeting points at  $(H_c, H_u) = (0, H_K/2)$  and  $(H_c, H_u) = (H_K/2, 0)$ . The spread about these peaks along the ridges gives rise to the “boomerang” shape noted by<sup>21</sup>.

As Fig. 3a shows,  $D_h f$  is antisymmetric about  $h_b = 0$  for all particle orientations. Therefore,  $B$  is also antisymmetric about  $H_b = 0$  or  $H_u = -H_c$ , as can be seen in Fig. 6b. By contrast,  $A$  is entirely on one side of this axis.

### C. Average over random orientations (anisotropic)

Suppose that some easy axis directions are more probable than others. In general this anisotropy can be described by a probability distribution of the form  $\nu(\theta, \phi; \boldsymbol{\kappa})$ , where  $\boldsymbol{\kappa}$  is a vector of distribution parameters. Since each easy axis has two directions, an integral of the FORC function over any half sphere should give the same average FORC function. This condition is satisfied if the distribution is bimodal:  $\nu(\pi - \theta, \phi; \boldsymbol{\kappa}) = \nu(\theta, \phi; \boldsymbol{\kappa})$ . One such distribution is the Bingham distribution<sup>17</sup>. In general, an integral over the Bingham distribution is messy. To give some insight into the effect of anisotropy I use a simple special case, a Dimroth-Watson distribution centered about the magnetic field direction<sup>17</sup>:

$$\nu(\theta; \kappa) = b(\kappa) \exp(\kappa \cos^2 \theta), \quad (22)$$

where

$$b(\kappa) = \left( 2 \int_0^1 \exp(\kappa t^2) dt \right)^{-1}. \quad (23)$$

When  $\kappa = 0$  this reduces to the isotropic distribution. If  $\kappa > 0$  the axes are concentrated around the field di-

rection ( $\theta = 0$ ) and if  $\kappa < 0$  they are more towards the perpendicular.

For a sample with this distribution (15) is replaced by

$$\tilde{\mu}(h_a, h_b; \kappa) = \int_0^{\pi/2} \tilde{\mu}(h_a, h_b; \theta) \nu(\theta; \kappa) \sin \theta d\theta. \quad (15c')$$

The calculation of  $\tilde{\mu}$  is similar to that in Section III B, and the result is the same except that (20c) is replaced by

$$g(\theta, h; \kappa) = f(\theta, h) \nu(\theta; \kappa) \sin \theta. \quad (20')$$

The anisotropy acts through the critical angle  $\theta_a \equiv \theta_s(h_a)$ , so it redistributes the FORC function in the  $h_a$  direction. However, the effect on the shape of the positive and negative peaks is not large because they are still strongly concentrated near  $H_u = H_K/2$  and  $H_c = H_K/2$ . The redistribution also depends on  $h_b$  because of (20b), changing the balance between  $A$  and  $B$ . The integral of  $A$  over the plane is

$$\begin{aligned} m_j &= \int_{-\infty}^{\infty} dh_a \int_{-\infty}^{\infty} \alpha(h_a) \delta(h_a + h_b) dh_b \\ &= \int_0^{\pi/2} f(\theta, h_s(\theta)) \nu(\theta; \kappa) \sin \theta d\theta. \end{aligned} \quad (24)$$

Since  $B$  is symmetric about  $h_b = 0$  its integral over the entire plane is zero. However, its integral over positive  $h_b$  is

$$m_{sl} = \int_0^{\pi/2} [f(\theta, 0) - f(\theta, h_s(\theta))] \nu(\theta; \kappa) \sin \theta d\theta, \quad (25)$$

while the integral over negative  $h_b$  is  $-m_{sl}$ . Now  $f(\theta, 0) = 2 \cos \theta$  is just the difference between the positive and negative remanences for a single particle. Its integral over  $\theta$  is  $m_j + m_{sl} = 2M_{rs}/M_s$ . Thus,  $m_j$  is the contribution of jumps to the total change in remanence while  $m_{sl}$  is the net effect of traveling up one curve and down another in each particle. Alternatively,  $m_j + m_{sl}$  and  $m_{sl}$  are the relative weights of the positive and negative regions.

The magnetizations  $m_j + m_{sl}$  and  $m_{sl}$  are shown in Fig. 7. The ratio  $M_{rs}/M_s$  increases monotonically with  $\kappa$  as the easy axes become more concentrated about the field direction. It is 0.5 at  $\kappa = 0$ , agreeing with the classic Stoner-Wohlfarth result for an isotropic sample, and it approaches unity as  $\kappa$  goes to infinity. Meanwhile  $m_{sl}$  has an absolute peak at  $\kappa = 0$ . This occurs because the isotropic distribution assigns the greatest weight to angles near  $45^\circ$ , and these are the angles for which  $f(\theta, 0) - f(\theta, h_s(\theta))$  is greatest (it is the difference between curves in Fig. 5). The negative peak is much smaller than the positive peak for prolate anisotropies, but it can be the bigger of the two for oblate anisotropies. For the same reason it should also be bigger if the anisotropy is prolate but centered around an axis perpendicular to the field.

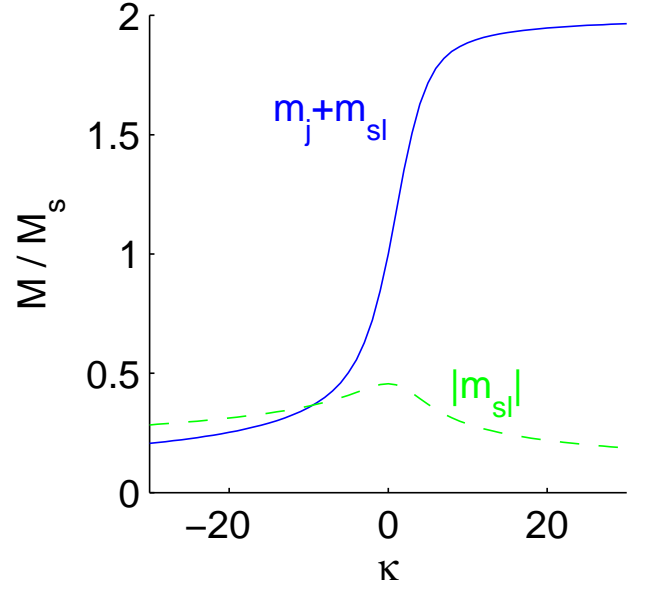


FIG. 7: The integrals of the FORC function over  $H_b > 0$  ( $m_j + m_{sl} = 2M_{rs}/M_s$ ) and  $H_b < 0$  ( $m_{sl}$ ) as a function of the Dimroth-Watson parameter  $\kappa$ .

#### D. Average over anisotropy field $H_K$

In a real material the magnetic particles are not identical. Suppose that the anisotropy field  $H_K$  varies. Let  $H_K = NM_s$ , where  $N$  is dimensionless.  $N$  may be the shape-dependent demagnetizing factor (Appendix A) or an effective demagnetizing factor representing magnetoelastic anisotropy. Suppose that  $N$  is always positive and has a probability density function  $\rho(N; \boldsymbol{\sigma})$ , where  $\boldsymbol{\sigma}$  is a vector of parameters. This pdf must satisfy  $\rho(N; \boldsymbol{\sigma}) \geq 0$  and  $\int_0^\infty \rho(N; \boldsymbol{\sigma}) dN = 1$ .

The FORC function is obtained by integrating the function for identical particles (9) over  $N$ :

$$\mu(H_a, H_b; \boldsymbol{\sigma}) = \frac{1}{M_s} \int_0^\infty \tilde{\mu}\left(\frac{H_a}{NM_s}, \frac{H_b}{NM_s}\right) \rho(N; \boldsymbol{\sigma}) \frac{dN}{N^2}. \quad (26)$$

The integrand is only nonzero for  $N_1 \leq N \leq N_2$ , where  $N_1 = |H_a|/M_s$  and  $N_2 = \min(1/2, 2|H_a|/M_s)$  (see Appendix A). The new coefficients are

$$A(H_a; \boldsymbol{\sigma}) = \int_{N_1}^{N_2} \alpha\left(\frac{H_a}{NM_s}\right) \rho(N; \boldsymbol{\sigma}) \frac{dN}{N} \quad (27a)$$

$$B(H_a, H_b; \boldsymbol{\sigma}) = \int_{N_1}^{N_2} \beta\left(\frac{H_a}{NM_s}, \frac{H_b}{NM_s}\right) \rho(N; \boldsymbol{\sigma}) \frac{dN}{N^2}. \quad (27b)$$

The theory in this article applies only to particles with uniaxial anisotropy, but many geologically interesting materials such as magnetite have a cubic magnetocrystalline anisotropy. Fortunately, the cubic anisotropy can

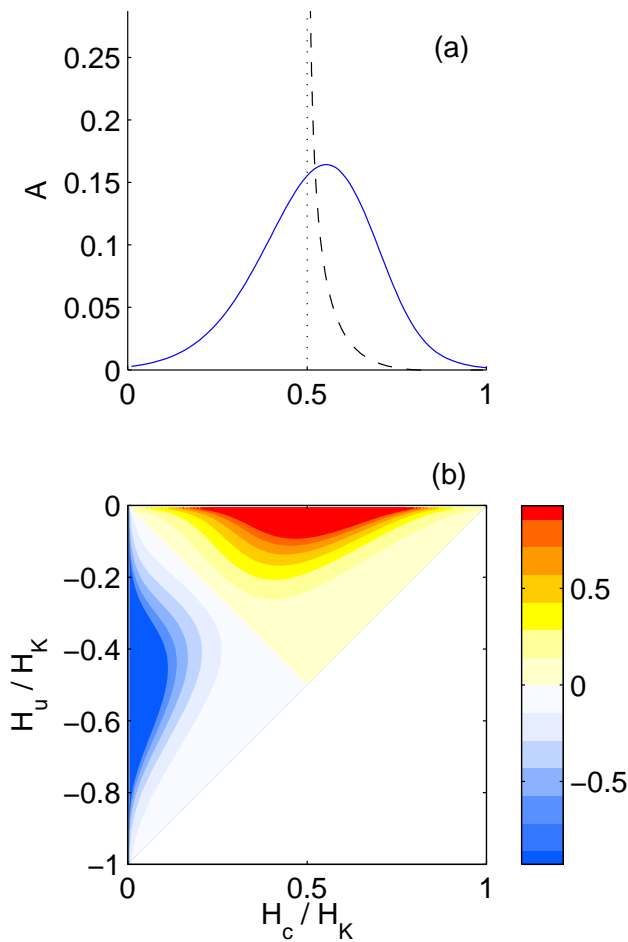


FIG. 8: The components of the FORC function an isotropic sample with a lognormal distribution of aspect ratios ( $\bar{q} = 2$  and  $\sigma = 0.25$ ). (a)  $A$ . The function for identical particles with aspect ratio  $\bar{q}$  is shown as a dashed line. (b)  $B$ . The same color scale is used as in Fig. 1b.

be neglected if the particles are elongated. For such particles it is best to start with a pdf for the particle aspect ratio  $q$  and use it to derive the pdf for the demagnetizing factor (Appendix A). The integral is evaluated using adaptive Gauss/Lobatto quadrature<sup>11</sup> with a relative accuracy of  $10^{-6}$  or better.

Many of the properties of a system of identical particles are still true of a system with a shape distribution. For example, in a set of identical particles,  $B(H_a, -H_b) = -B(H_a, H_b)$ . In (27) this implies that  $B(H_a, -H_b; \sigma) = -B(H_a, H_b; \sigma)$ . Thus, the antisymmetry of  $B$  about  $H_u = -H_c$  is preserved. Also, the positive and negative peaks have the same relative weights as in Section III C.

The arguments are plotted in Fig. 8 for a lognormal distribution of aspect ratios with mean  $\bar{q} = 2$ , corresponding to a demagnetizing factor  $N_0(\bar{q}) = 0.24$ . Equation 27b predicts that the shape distribution will spread the FORC function equally in all directions, and this is consistent with Fig. 8. One result of this spreading is

that the slanted ridges are replaced by humps that are roughly symmetric about the peaks.

#### IV. DISCUSSION

This model makes two kinds of predictions about FORC functions of uniaxial SD particles. Some predictions follow directly from the properties of the single-particle hysteresis loops. These include the negative region near the  $H_u$  axis, the positive region near the  $H_c$  axis, the delta function on the  $H_c$  axis, and the equal distances of these peaks from the origin. Also, the FORC function is identically zero for  $H_u > 0$ . These predictions are robust because they do not depend on the distribution of particle orientations or shapes. The other kind of prediction does depend on these distributions. The distribution of particle orientations has little effect on the shapes of the positive and negative peaks, but it has a strong effect on the relative size of these peaks. The distribution of particle shapes affects the shapes of the peaks equally, with a realistic distribution tending to smear them out and remove the ridge between the peaks.

In this section I discuss two robust predictions and their significance. The first, a negative peak near the  $H_u$  axis, is one of the surprises to come out of plots of experimental FORC functions. I clarify its physical significance in section IV A. The second is that the function is identically zero for  $H_u > 0$ . This obviously violates the symmetry  $\mu(-H_c, H_u) = \mu(H_c, H_u)$  required by classical Preisach theory<sup>18</sup>. In section IV B I discuss this symmetry violation and its relationship to the dual definition of  $\mu$  for increasing and decreasing FORCs. Finally, in section IV C I discuss the possible reasons why FORC functions of real samples always have nonzero values for  $H_u > 0$ .

##### A. Negative parts of the FORC function

As mentioned in Section I, Preisach modelers often assume that the Preisach function is a probability density. However, this assumption is contradicted by the negative region in Fig. 1b and in other single-domain samples<sup>1,29</sup>. The negative region does not violate any necessary condition for Preisach theory. Indeed, negative Preisach functions can be related to observable features of first-order reversal curves<sup>18</sup>.

Preisach theory represents hysteresis as the weighted sum of rectangular hysteresis loops called hysterons. Each hysteron has an “up” and a “down” state with outputs of +1 and -1. A hysteron associated with the point  $(H_1, H_2)$  has a downward jump at  $H_1$  and an upward jump at  $H_2$ . The FORC function at  $(H_1, H_2)$  is the weight assigned to that hysteron.

A negatively weighted hysteron is simply an upside-down hysteresis loop, having an upward jump for decreasing field and a downward jump for increasing field.

Those familiar with Preisach theory may find this disturbing because a particle with a negative hysteresis loop would perform net work on the field, violating the law of conservation of energy. However, the hysteresis loop for a Stoner-Wohlfarth particle is represented by a distribution of hysterons, and in a circuit around the loop the field does net work on the particle. Negatively weighted hysterons are a reminder that the hysterons do not have a simple physical meaning.

The negative part of  $A$  comes from jumps in the direction of the field, as in Fig. 4. This only occurs in particles with easy axes nearly perpendicular to the field. The negative part of  $B$  comes from the difference in slopes near a jump. Almost all particles contribute to  $B$  (the exception being those with easy axes parallel to the field). As the field approaches a jump the slope of the magnetization curve increases to infinity. After the jump the slope is finite again. If the jump is from a lower curve to an upper curve ( $H_b = -H_a$  in the Stoner-Wohlfarth model), the FORC function approaches positive infinity at the jump. If the jump is the other way ( $H_b = H_a$ ), the FORC function approaches negative infinity. (A similar interpretation was offered by<sup>28</sup>, but it was based on a hypothetical form for a hysteron and there was no approach to infinity.)

The approach to infinity of the slope is a “generic” property of instabilities that occurs in many physical systems<sup>14</sup> and has been documented in micromagnetic models<sup>13,24,25</sup>. It is associated with a bifurcation at which a stable state and an energy barrier converge and annihilate each other. Thus, in any magnetic system the difference between slopes should always make a negative contribution to the FORC function.

If there is always a negative contribution to the FORC function near  $H_a = H_b$ , why is it not seen in all experimental FORC diagrams? In larger particles it may be canceled out by small positive jumps. In larger particles large jumps are replaced by small Barkhausen jumps due to movement of domain walls over defects. In a system with many particles there is always an upward jump near any downward jump. Downward jumps contribute to the FORC function only through the difference in slopes, but upward jumps also contribute the height of the jump. Thus, the upward jumps hide the lower jumps and only a positive contribution is seen.

## B. The FORC function violates Preisach symmetry

Classical Preisach theory requires that the FORC function have the symmetry

$$\mu(-H_b, -H_a) = \mu(H_a, H_b), \quad (28)$$

which is a reflection symmetry about the  $H_c$  axis on a FORC diagram. FORC functions of real samples often do not have this symmetry. Why is the symmetry broken?

In Fig. 2 the upper and lower branches of the main loop are images of each other under inversion symme-

try. For each point  $(H, M)$  on the upper curve there is a point  $(-H, -M)$  on the lower curve. This symmetry follows from the invariance of Maxwell’s equations under time reversal<sup>15</sup>. Similarly, for each point  $M^i(H_a, H_b)$  on an increasing FORC there is a point  $M^d(-H_b, -H_a) = -M^i(H_a, H_b)$  on a decreasing FORC. If we label the increasing FORC function  $\mu^i$  and the decreasing FORC function  $\mu^d$ , it follows from (1,2) that  $\mu^i(-H_b, -H_a) = \mu^d(H_a, H_b)$ . Thus, the increasing and decreasing FORC functions are related by reflection in the  $H_c$  axis. (Such a symmetry can be seen, for example, between the left halves of Fig. 5 in<sup>12</sup>.) The FORC functions are identical if and only if they have the Preisach symmetry (28).

Between a given pair of fields the increasing and decreasing FORCs should have the same shape because the same hysterons contribute to the change. This is a special case of the congruency property<sup>18</sup>. However, they do not have the same shape for most single-particle hysteresis loops. In Fig. 3, for  $-h_s < h_a < h_b < h_s$  the increasing FORCs are on the upper curve while the decreasing FORCs are on the lower curve. These curves have different slopes everywhere except at  $h = 0$ . Thus, the symmetry breaking is due to the difference in slope. Because of the difference in slope, classical Preisach theory cannot represent Stoner-Wohlfarth hysteresis<sup>18</sup>.

The difference in slopes is represented by component  $B$  in the FORC function. The FORC function does not contain information on the slope of either curve by itself or on the saturation magnetization. This information loss occurs because the FORC function is obtained by taking two derivatives of the magnetization  $M(H_a, H_b)$ . To recover  $M$  one must integrate twice, which introduces two unknown integration constants. However, the information loss has an advantage. Paramagnetic and superparamagnetic components are removed, isolating the hysteresis. The FORC function also highlights regions where the hysteresis has a large effect on the magnetization.

## C. Why are real FORC functions nonzero for $H_u > 0$ ?

The greatest disagreement between the theoretical FORC function derived in this article and the experimental FORC function in Fig. 1 is the spread of the positive peak to positive  $H_u$ . Indeed, all experimental FORC functions have a nonzero region for  $H_u > 0$ . This is to be expected if the samples are not SD, but the magnetic tape is composed of SD particles.

One possible explanation for the spread of the peak is a numerical artifact. Experimental functions are based on polynomial fits to discrete measurements of  $M(H_a, H_b)$ . The field increments must be very small to represent some of the features of Stoner-Wohlfarth systems. Half the change in magnetic remanence occurs between  $H = 0.5H_K$  and  $H = 0.524H_K$ , the latter being the coercivity

of remanence<sup>38</sup>. Experimental FORC functions are derived from polynomial fits to  $(2 * SF + 1)^2$  points, where SF is called the smoothing factor. The same procedure is used by<sup>21</sup> to fit a FORC function to numerical simulations of FORC curves for Stoner-Wohlfarth particles. They get a positive peak that is nearly symmetric about the  $H_c$  axis, aside from the boomerang shape of the lowest contours. Since the true FORC function for Stoner-Wohlfarth particles is zero for  $H_u > 0$ , the spreading of the peak in their model must be a numerical artifact.

Numerical artifacts are probably not the reason for the spread of the peak in Fig. 1b. The FORC function looks essentially the same for  $SF = 1$  and  $SF = 5$ , aside from small-scale noise. Thus, the spread of the positive peak to  $H_u > 0$  is probably due to a physical effect.

Three physical effects could give rise to some spreading. First, thermal fluctuations make jumps occur early<sup>27</sup>. This effect narrows hysteresis loops, which would move the FORC function to lower  $H_c$ . It also replaces a jump at a discrete switching field by a probability of a jump that increases continuously as the field approaches the switching field. Since the positive peak relates the upward jump to the downward jump, and both jumps spread independently, thermal fluctuations should spread the positive peak equally in the  $H_c$  and  $H_u$  directions. By contrast, the negative peak should spread mainly in the  $H_a$  direction. Thermal fluctuations could account for some of the observed spreading, but the effect is probably too small. A large thermal effect would imply a strong temperature dependence of the FORC function, and the temperature dependence of the FORC functions in<sup>1</sup> is very weak. It is weak because probability distribution is generally tightly concentrated around an effective switching field. Compared to zero fluctuations, the switching field is reduced by a factor  $1 - (V_{SP}/V)^x$ , where  $V_{SP}$  is the upper volume limit for superparamagnetism and  $x$  is between 1.43 and 2<sup>27</sup>. The reduction is already less than 5% for a particle that is only twice the superparamagnetic limit in each dimension. The extent of spreading will be even less.

Second, particle interactions can spread the FORC function in the  $H_u$  direction without having much effect on the  $H_c$  direction<sup>21</sup>. Although this could account for some of the spreading in Fig. 1b, particle interactions are undesirable in magnetic tapes. Thus, manufacturers try to keep the magnetic particles apart to reduce interactions.

Whether or not particle interactions are present, a third effect is unavoidable: non-SD magnetization change. The ratio  $M_{rs}/M_s = 0.62$  is strong evidence for an SD saturation remanence, but that does not mean that the particle reverses by the SD mechanism of uniform rotation. Indeed, uniform rotation is unlikely.<sup>23</sup> calculated the upper size limit for uniform rotation and showed that it is never far from the upper limit for superparamagnetism, even when the size range for SD saturation remanence is broad.

A particle with an SD saturation remanent state can

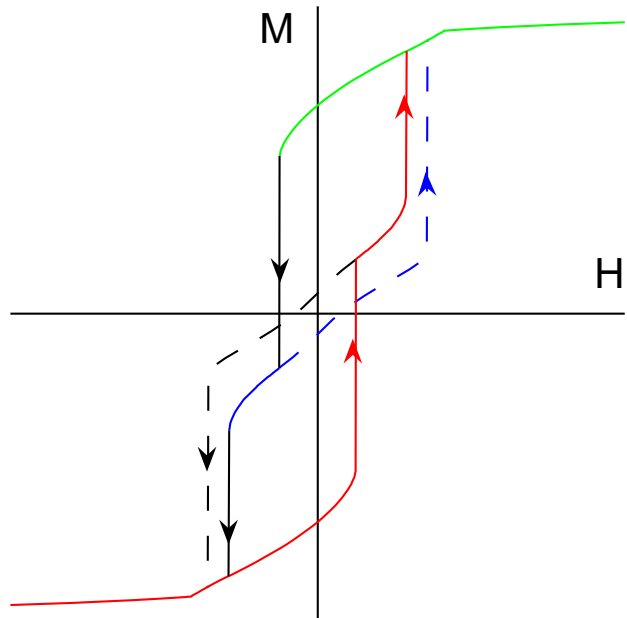


FIG. 9: The magnetic hysteresis for a magnetite particle with volume  $(0.09 \text{ m})^3$ , a triaxial shape  $X = 1.5Y = 1.4Z$  and a field in the  $(8, 4, 1)$  direction. Arrows show the direction of jumps. The solid curve is the main hysteresis loop while the dashed lines are FORCs for fields after the first jump. The increasing FORCs are highlighted in green, blue and red. Adapted from Fig. 11 in<sup>24</sup>.

also have a non-SD, or multidomain (MD), remanence after partial demagnetization.<sup>24</sup> showed that when a MD state has the lowest energy, new jumps and new loops appear in the hysteresis (indeed, these were the first micromagnetic simulations of FORCs). An example is shown in Fig. 9. In this example the saturation remanent state is not SD, but that is because the particle is not very elongated. There are three increasing FORCs, one for any field  $H_a$  before the first jump (green), one for any  $H_a$  between jumps (blue) and one after the second jump (red). Considering just the contribution of the jumps to the FORC function, the difference between the green and blue curves will contribute a delta function with  $H_u > 0$ . The difference between blue and red curves will contribute one delta function with  $H_u < 0$  (first red jump) and one with  $H_u = 0$  (second jump). The overall spreading is nearly symmetric, as one would expect of a system that has inversion symmetry in the  $(\mathbf{H}, \mathbf{M})$  plane (section IV B).

## V. CONCLUSIONS

The FORC function of a system of noninteracting, elongated single-domain particles has some robust properties. It has two parts. A delta function on the  $H_c$  axis represents jumps in magnetization. A continuous function over  $H_c > 0$  and  $H_u < 0$  represents differences in

slopes between the upper and lower magnetization curves for each particle. The latter has a positive peak on the  $H_c$  axis and a negative peak on the negative  $H_u$  axis. These peaks are at equal distances from the origin.

There are also some properties that depend on the distribution of particle orientations and shapes. If the particles are identical, each peak has a “boomerang” shape with a  $135^\circ$  internal angle. This shape is due to the strong dependence of the switching field on the angle between the easy axis and the field when that angle is near  $45^\circ$ . The relative size of the negative and positive peaks depends on the distribution of easy axis orientations. If the distribution is weighted parallel to the field the positive peak is dominant, but if the distribution is weighted perpendicular to the field the negative peak is slightly larger. If the particles are not identical, the peaks become broader and the “boomerang” shape is replaced by a hump that is more nearly symmetrical about the highest point.

The negative region is consistent with classical Preisach theory but inconsistent with assumptions that the FORC function is a probability distribution. It seems to violate conservation of energy, but on closer examination it does not. It is due to the difference between slopes before and after each downward jump. This effect should make a negative contribution to the FORC function of all particles. The negative region is probably not seen in larger particles because it is canceled by nearby upward jumps.

The theory predicts that the FORC function should be zero for  $H_u > 0$ , but experimental FORC functions for SD particles are always nonzero on both sides of the  $H_c$  axis. The disagreement is probably due to a combination of particle interactions and multidomain remanent states. The latter can occur even in nominally SD particles. It is not apparent in the ratio  $M_{rs}/M_s$  because the saturation magnetization state is SD.

### APPENDIX A: A PROBABILITY DENSITY FUNCTION FOR THE DEMAGNETIZING FACTOR

In this Appendix I derive an expression for the probability density function (pdf) of the demagnetizing factor  $N$  given a probability function for the aspect ratio of a spheroid. The aspect ratio is defined as  $q = a/b$ , where  $a$  is the major axis and  $b$  is the minor axis of the ellipsoid. For a prolate ellipsoid the demagnetizing factor is given by<sup>2</sup>

$$N = \frac{1}{2} - \frac{3}{2}q(q^2 - 1)^{-3/2} \cosh^{-1} q - \frac{3}{2}(q^2 - 1)^{-1}. \quad (\text{A1})$$

As  $q$  goes from one to infinity,  $N$  starts at zero and approaches an asymptote of  $1/2$ . I ignore  $q < 1$  (an oblate spheroid) because it has an easy plane instead of an easy axis and Stoner-Wohlfarth theory does not apply.

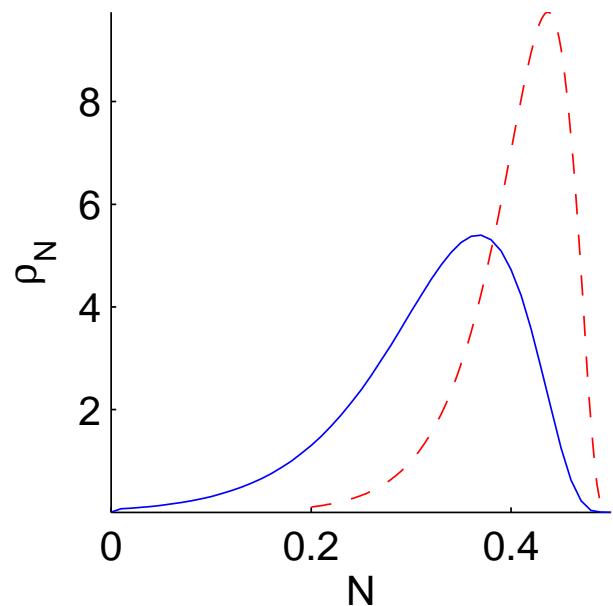


FIG. 10: Probability density functions for the demagnetizing factor  $N$  derived from lognormal densities of the grain aspect ratio  $q$ . The solid and dashed lines both have the same standard deviation  $\sigma = 0.4$ , but the pdf for  $\bar{q} = 5$  (solid line) is narrower than the pdf for  $\bar{q} = 3$  (dashed line) because  $N$  approaches a limit of 0.5 for large  $q$ .

Suppose that the aspect ratio  $q$  has a pdf  $\rho_q(q; \sigma)$  such that  $\rho_q$  is negligible for  $q < 1$ . The corresponding pdf for the demagnetizing factor is given by<sup>31</sup>

$$\rho(N; \sigma) = \frac{1}{|N'(q(N))|} \rho_q(q(N); \sigma), \quad (\text{A2})$$

where  $q(N)$  is the inverse of the function  $N(q)$  and  $N'(q)$  is the first derivative of  $N(q)$ .

In evaluating the integrals in (27), one must take care to restrict  $H_a$  and  $H_b$  to the region where the density is nonzero. Otherwise,  $N$  can be out of bounds and  $q(N)$  will be undefined. Combining the integral limits  $-1 \leq h \leq -1/2$  with  $0 \leq N \leq 1/2$  and  $h = H_a/NM_s$ , we get  $-M_s/2 \leq H_a \leq 0$ . In addition the upper integral limit must be changed to  $N_2 = \min(1/2, 2|H_a|/M_s)$ . Finally,  $|H_b| \leq |H_a|$ . Outside of this region the FORC function is zero.

An example of functions  $\rho_N$  generated using a lognormal function  $\rho_q(N; \bar{q}, \sigma)$  is plotted in Fig. 10. Because  $N$  approaches a limit of 0.5 as  $q$  approaches infinity,  $\rho_N$  gets narrower as the mean  $q$  increases even if the standard deviation remains the same. The distribution is also skewed upwards.

### ACKNOWLEDGMENTS

I would like to thank Chris Pike for many valuable comments on this manuscript and for the magnetic

tape data. Reviews by Adrian Muxworthy, Stephen Park, Claire Carvallo, Andy Jackson and an anonymous reviewer also led to significant improvements in the manuscript.

Wiley & Sons, translated from the French by G. M. Temmer. 1136 pp.

- 
- \* Andrew\_Newell@ncsu.edu; <http://www4.ncsu.edu/~ajnewell/index.html>
- <sup>1</sup> Carvallo, C., O. Özdemir, and D. J. Dunlop (2004), First-order reversal curve (FORC) diagrams of elongated single-domain grains at high and low temperatures, *J. Geophys. Res.*, *109*, B04,105, doi:10.1029/2003JB002539.
  - <sup>2</sup> Chikazumi, S. (1997), *Physics of Ferromagnetism*, Oxford, New York, 655 pp.
  - <sup>3</sup> Day, R., M. Fuller, and V. A. Schmidt (1977), Hysteresis properties of titanomagnetites: grain-size and compositional dependence, *Phys. Earth Planet. Inter.*, *13*, 260–267.
  - <sup>4</sup> Dunlop, D. J. (1969), Hysteretic properties of synthetic and natural monodomain grains, *Phil. Mag.*, *19*, 329–338.
  - <sup>5</sup> Dunlop, D. J. (2002), Theory and application of the Day plot ( $M_{rs}/M_s$  versus  $H_{cr}/H_c$ ) 1. Theoretical curves and tests using titanomagnetite data, *J. Geophys. Res.*, *107*(B3), 2056, doi:10.1029/2001JB000486.
  - <sup>6</sup> Dunlop, D. J. (2002), Theory and application of the Day plot ( $M_{rs}/M_s$  versus  $H_{cr}/H_c$ ) 2. Application to data for rocks, sediments, and soils, *J. Geophys. Res.*, *107*(B3), 2057, doi:10.1029/2001JB000487.
  - <sup>7</sup> Dunlop, D. J., and O. Özdemir (1997), *Rock Magnetism: Fundamentals and Frontiers*, Cambridge Univ. Press, New York, 573 pp.
  - <sup>8</sup> Dunlop, D. J., M. F. Westcott-Lewis, and M. E. Bailey (1990), Preisach diagrams and anhysteresis: do they measure interactions?, *Phys. Earth Planet. Inter.*, *65*, 62–77.
  - <sup>9</sup> Egli, R. (2003), Analysis of the field dependence of remanent magnetization curves, *J. Geophys. Res.*, *108*, 2081, doi:10.1029/2002JB002023.
  - <sup>10</sup> Feinberg, J. M., H. R. Wenk, P. R. Renne, and G. R. Scott (2004), Epitaxial relationships of clinopyroxene-hosted magnetite determined using electron backscatter diffraction (EBSD) technique, *Am. Mineral.*, *89*, 462–466.
  - <sup>11</sup> Gander, W., and W. Gautschi (2000), Adaptive quadrature - revisited, *BIT*, *40*(1), 84–101.
  - <sup>12</sup> Hejda, P., and T. Zelinka (1990), Modelling of hysteresis processes in magnetic rock samples using the Preisach diagram, *Phys. Earth Planet. Inter.*, *63*, 32–40.
  - <sup>13</sup> Hubert, A., and W. Rave (1999), Systematic analysis of micromagnetic switching processes, *phys. stat. sol. (b)*, *211*, 815–829.
  - <sup>14</sup> Iooss, G., and D. D. Joseph (1990), *Elementary Stability and Bifurcation Theory*, 2nd ed., Springer-Verlag, New York, 324 pp.
  - <sup>15</sup> Jackson, J. D. (1975), *Classical Electrodynamics*, John Wiley and Sons, 848 pp.
  - <sup>16</sup> Jackson, M. (1990), Diagenetic sources of stable remanence in remagnetized Paleozoic cratonic carbonates: A rock magnetic study, *J. Geophys. Res.*, *95*, 2753–2761.
  - <sup>17</sup> Mardia, K. V. (1972), *Statistics of Directional Data*, Academic Press, New York, NY, 357 pp.
  - <sup>18</sup> Mayergoyz, I. D. (1991), *Mathematical Models of Hysteresis*, Springer-Verlag.
  - <sup>19</sup> Mee, C. D., and E. D. Daniel (Eds.) (1996), *Magnetic Storage Handbook*, 2nd ed., McGraw-Hill.
  - <sup>20</sup> Messiah, A. (c1962), *Quantum Mechanics*, vol. 1-2, John Wiley & Sons, translated from the French by G. M. Temmer. 1136 pp.
  - <sup>21</sup> Muxworthy, A., D. Heslop, and W. Williams (2004), Influence of magnetostatic interactions on first-order-reversal-curve (FORC) diagrams: a micromagnetic approach, *Geophys. J. Int.*, *158*, 888–897, doi:10.1111/j.1365-246X.2004.02358.x.
  - <sup>22</sup> Muxworthy, A. R., and D. J. Dunlop (2002), First-order reversal curve (FORC) diagrams for pseudo-single-domain magnetites at high temperature, *Earth Planet. Sci. Lett.*, *203*, 369–382.
  - <sup>23</sup> Newell, A. J., and R. T. Merrill (1999), Single-domain critical sizes for coercivity and remanence, *J. Geophys. Res.*, *104*, 617–628.
  - <sup>24</sup> Newell, A. J., and R. T. Merrill (2000), Nucleation and stability of remanent states, *J. Geophys. Res.*, *105*, 19,377–19,391.
  - <sup>25</sup> Newell, A. J., and R. T. Merrill (2000), Size dependence of hysteresis properties of small pseudo-single-domain grains, *J. Geophys. Res.*, *105*, 19,393–19,403.
  - <sup>26</sup> Parry, L. G. (1982), Magnetization of immobilized particle dispersions with two distinct particle sizes, *Phys. Earth Planet. Inter.*, *28*, 230–241.
  - <sup>27</sup> Pfeiffer, H. (1990), Determination of anisotropy field distribution in particle assemblies taking into account thermal fluctuations, *phys. status. solidi. A*, *118*, 295–306.
  - <sup>28</sup> Pike, C. R. (2003), First-order reversal-curve diagrams and reversible magnetization, *Phys. Rev. B*, *68*, 104,424.
  - <sup>29</sup> Pike, C. R., A. P. Roberts, and K. L. Verosub (1999), Characterizing interactions in fine magnetic particle systems using first order reversal curves, *J. Appl. Phys.*, *85*, 6660–6667.
  - <sup>30</sup> Pike, C. R., A. P. Roberts, M. J. Dekkers, and K. L. Verosub (2001), An investigation of multi-domain hysteresis mechanisms using FORC diagrams, *Phys. Earth Planet. Inter.*, *126*, 11–25.
  - <sup>31</sup> Rice, J. A. (1995), *Mathematical Statistics and Data Analysis*, 2nd ed., Duxbury Press, Belmont, CA.
  - <sup>32</sup> Roberts, A. P., C. R. Pike, and K. L. Verosub (2000), First-order reversal curve diagrams: A new tool for characterizing the magnetic properties of natural samples, *J. Geophys. Res.*, *105*, 29,461–28,475.
  - <sup>33</sup> Robertson, D. J., and D. E. France (1994), Discrimination of remanence-carrying minerals in mixtures, using isothermal remanent magnetisation acquisition curves, *Phys. Earth Planet. Inter.*, *82*, 223–234.
  - <sup>34</sup> Selkin, P. A., J. S. Gee, L. Tauxe, W. P. Meurer, and A. J. Newell (2000), The effect of remanence anisotropy on paleointensity estimates: a case study from the Archean Stillwater Complex, *Earth Planet. Sci. Lett.*, *183*(3–4), 403–416.
  - <sup>35</sup> Song, T., and R. M. Roshko (2000), A Preisach model for systems with magnetic order, *Physica B*, pp. 24–27.
  - <sup>36</sup> Spivak, M. (1967), *Calculus*, Benjamin/Cummings, London.
  - <sup>37</sup> Stancu, A., C. Pike, L. Stoleriu, P. Postolache, and D. Cimpoesu (2003), Micromagnetic and Preisach analysis of the

- First Order Reversal Curves (FORC) diagram, *J. Appl. Phys.*, *93*(10), 6620–6622.
- <sup>38</sup> Stoner, E. C., and E. P. Wohlfarth (1948), A mechanism of magnetic hysteresis in heterogeneous alloys, *Philos. Trans. R. Soc. London Ser. A*, *240*, 599–642.
- <sup>39</sup> Tauxe, L., T. A. T. Mullender, and T. Pick (1996), Potbellies, wasp-waists, and superparamagnetism in magnetic hysteresis, *J. Geophys. Res.*, *101*, 571–583.
- <sup>40</sup> Vajda, F., and E. Della Torre (1991), Measurements of output-dependent Preisach functions, *IEEE Trans. Magn.*, *27*(6), 4757–4762.
- <sup>41</sup> Worm, H.-U., and M. Jackson (1999), The superparamagnetism of Yucca Mountain Tuff, *J. Geophys. Res.*, *104*(B11), 25,415–25,425.